European Congress on Computational Methods in Applied Sciences and Engineering
ECCOMAS Computational Fluid Dynamics Conference 2001
Swansea, Wales, UK, 4-7 September 2001

HYBRID LES-RANS: A COMBINATION OF A ONE-EQUATION SGS MODEL AND A $K-\omega$ MODEL FOR PREDICTING RECIRCULATING FLOWS

Lars Davidson

Dept. of Thermo and Fluid Dynamics, Chalmers University of Technology, SE-412 96 Göteborg, Sweden, e-mail: lada@tfd.chalmers.se, web page: http://www.tfd.chalmers.se/~lada

Key words: LES, hybrid models, zonal models, LES-RANS, DES

Abstract. *A hybrid LES-RANS model is proposed. RANS is used in the near wall regions ($y^+ \lesssim 60$), and the turbulence is modelled with a $k-\omega$ model. LES is used in the remaining part of the flow, and the SGS turbulence is modelled with a one-equation k_{sgs} model. The same continuity and momentum equations are solved throughout the domain, the only difference being that the turbulent viscosity is taken from the $k-\omega$ model in the RANS region, and from the one-equation k_{sgs} model in the LES region. The new model is applied to two incompressible flow test cases. They are fully developed flow in a plane channel and the flow over a 2D-hill in a channel.*

1 Introduction

With LES very fine grids must be employed in all three directions. The near-wall grid spacing should be about $y^+ \simeq 1$ in the wall-normal direction. This is similar to the requirement in RANS using low-Re number models. Contrary to RANS, with LES a fine grid must also be used in the spanwise (z) and streamwise (x) directions. This enables resolution of the near-wall turbulent structures in the viscous sublayer and the buffer layer (streaks), which are responsible for the major part of the turbulence production. The requirement for a well-resolved LES on Δx^+ and Δz^+ in the near-wall region is approximately 100 and 20, respectively [1]. In the fully turbulent region, say for $y^+ > 50$, coarser grid spacing can probably be used. In this region Δx^+ and Δz^+ are presumably dictated by the requirement of resolving the mean flow rather than the near-wall turbulent processes.

In this work, coupling a two-equation $k-\omega$ model in the near-wall region (RANS region) with a one-equation k_{sgs} model in the core region (LES region) is proposed, see Fig. 1a. The momentum equations are solved throughout the computational domain. The turbulent RANS viscosity from the $k-\omega$ model is used in the RANS region, and the turbulent SGS viscosity from the one-equation model is used in the LES region. For simplicity, the matching line between the RANS and LES region is presently defined at a pre-selected grid line.

This approach is in a way similar to that used in DES (Detached Eddy Simulation) [2–5]. One difference is that whereas in DES the object is to model the turbulent boundary layer with RANS; only the detached eddies in the outer boundary layer is modelled with LES. In the present hybrid LES-RANS, the matching line is located somewhere in the logarithmic part of the boundary layer.

2 Equations

The Navier-Stokes, time-averaged in the near-wall regions and filtered in the core region, reads

$$\frac{\partial \bar{u}_i}{\partial t} + \frac{\partial}{\partial x_j}\left(\bar{u}_i \bar{u}_j\right) = \beta \delta_{1j} - \frac{1}{\rho}\frac{\partial \bar{p}}{\partial x_i} + \frac{\partial}{\partial x_j}\left[(\nu + \nu_T)\frac{\partial \bar{u}}{\partial x_j}\right] \tag{1}$$

$$\frac{\partial \bar{u}_i}{\partial x_i} = 0 \tag{2}$$

where $\nu_T = \nu_t$ for $y \le y_{ml}$, otherwise $\nu_T = \nu_{sgs}$. Furthermore, the bar ($\bar{.}$) over the velocity components and pressure denote time averaging in the RANS region and filtering in the LES region. An alternative interpretation is that the bar denotes filtering in both regions, but that the SGS length scale in the near-wall region is defined k and ω, and in the core region from the usual cell size. For more discussion, see Sub-section 4.3.

Case	z_{max}	y_{ml}/δ	j_{match}	y^+_{ml}	Δz^+
1	π	0.023	4	25	104
2	π	0.057	8	60	104
3	2π	0.057	8	60	208
4	π	0	0	0	104

Table 1: Channel flow, $Re_\tau = 1050$, $x_{max} = 4\pi$ ($\Delta x^+ = 412$). Size of the computational domain and position of the matching line (y_{ml}) between the LES and RANS regions. The j_{match} value represents number of cells in the RANS region. Note that only LES is used in Case 4.

For both the channel flow and the hill flow, periodic boundary conditions are used in the streamwise and spanwise directions. No slip conditions are used at the walls in the channel flow, and at the lower wall in the hill flow. At the upper hill flow wall, because the resolution is here rather poor ($y^+ \approx 30$ for the first node), wall functions are used based on the instantaneous log law. It was found that computed results are insensitive to the choice of boundary conditions at the upper wall (wall functions or no-slip conditions).

The first term on the right-hand side of Eq. 1 represents the streamwise driving pressure term, both in the channel flow and the hill flow. In the former case the Reynolds number based on the wall-friction velocity Re_τ is prescribed, and thus $\beta = 1$. For the hill flow, in order to get the correct bulk flow different values of β are tested. A value of $\beta = 2$ is finally chosen which is kept constant in all hill computations (the same value was used in [**?**]).

3 The Hybrid LES–RANS model

A $k-\omega$ model [9] is used in the near-wall layer, and the one-equation SGS model by Yoshizawa [10] for the core region. The $k-\omega$ model is formulated as

$$\begin{aligned}
\frac{\partial k}{\partial t} + \frac{\partial}{\partial x_j}(\bar{u}_j k) &= \frac{\partial}{\partial x_j}\left[\left(\nu + \frac{\nu_t}{\sigma_k}\right)\frac{\partial k}{\partial x_j}\right] + P_k - c_k f_k \omega k \\
\frac{\partial \omega}{\partial t} + \frac{\partial}{\partial x_j}(\bar{u}_j \omega) &= \frac{\partial}{\partial x_j}\left[\left(\nu + \frac{\nu_t}{\sigma_\omega}\right)\frac{\partial \omega}{\partial x_j}\right] + \frac{\omega}{k}\left(c_{\omega 1} f_\omega P_k - c_{\omega 2} k\omega\right) + c_\omega \frac{\nu_t}{k}\left(\frac{\partial k}{\partial x_j}\frac{\partial \omega}{\partial x_j}\right) \\
\nu_t = f_\mu \frac{k}{\omega},\ P_k &= 2\nu_t \bar{S}_{ij}\bar{S}_{ij},\ \bar{S}_{ij} = \frac{1}{2}\left(\frac{\partial \bar{u}_i}{\partial x_j} + \frac{\partial \bar{u}_j}{\partial x_i}\right)
\end{aligned} \tag{3}$$

The model of Yoshizawa reads

$$\begin{aligned}
\frac{\partial k_{sgs}}{\partial t} + \frac{\partial}{\partial x_j}(\bar{u}_j k_{sgs}) &= \frac{\partial}{\partial x_j}\left[(\nu + \nu_{sgs})\frac{\partial k_{sgs}}{\partial x_j}\right] + P_{k_{sgs}} - C_\varepsilon \frac{k_{sgs}^{3/2}}{\Delta} \\
\nu_{sgs} = C_k \Delta k_{sgs}^{1/2},\ P_{k_{sgs}} &= 2\nu_{sgs}\bar{S}_{ij}\bar{S}_{ij} \\
\Delta = \min\left\{\Delta_\xi, \Delta_\eta, \Delta_\zeta\right\},\ C_k = 0.07,\ C_\varepsilon &= 1.05
\end{aligned} \tag{4}$$

where ξ, η and ζ denote the three coordinate directions defined by a general curvilinear grid. The turbulent kinetic energy in the RANS region ($y \leq y_{ml}$) is denoted by k, and the SGS turbulent kinetic energy in the LES region ($y > y_{ml}$) by k_{sgs}. The coefficients have been assigned slightly different values [11] than in the original model. Note that, contrary to the standard Yoshizawa model, in which $\Delta = (\Delta_\xi \Delta_\eta \Delta_\zeta)^{1/3}$, here the smallest cell side is used. This is was found to considerably improve predictions.

The matching line near the lower wall is located at y_{ml} (see Fig. 1a). The subscript j_{match} is used here to denote the cell below the matching line y_{ml}. At the matching line, the following ω interface condition is used:

$$j = j_{match} : \ \frac{\partial \omega}{\partial y} = 0 \tag{5}$$

Contrary to [**?**], no interface condition is used for k and k_{sgs}. These quantities are simply transported in a natural way by convection-diffusion over the matching line.

3.1 The Numerical Method

An implicit, two-step time-advancement methods is used. The discrete form of Eq. 1 can be written as

$$\bar{u}_i^{n+1/2} = \bar{u}_i^n + \Delta t H\left(u_i^n, u_i^{n+1/2}\right) - \frac{1}{\rho}\alpha \Delta t \frac{\partial p^{n+1}}{\partial x_i} - \frac{1}{\rho}(1-\alpha)\Delta t \frac{\partial p^n}{\partial x_i} \tag{6}$$

where $H\left(u_i^n, u^{n+1/2}\right)$ includes convection and the viscous and subgrid stresses, and $\alpha = 0.5$ (Crank-Nicolson). Equation 6 gives $\bar{u}_i^{n+1/2}$ which does not satisfy continuity. An intermediate velocity field is computed by subtracting the implicit part of the pressure gradient, i.e.

$$\bar{u}_i^* = \bar{u}_i^{n+1/2} + \frac{1}{\rho}\alpha \Delta t \frac{\partial p^{n+1}}{\partial x_i}. \tag{7}$$

Now $\bar{u}_i^{n+1/2}$ in Eq. 7 is replaced by the final velocity field at level $n+1$, i.e. $\bar{u}_i^{n+1}$. Taking the divergence of Eq. 7, requiring that the face velocities $\bar{u}_{i,f}^{n+1}$ (which are obtained by linear interpolation) satisfy the continuity equation the following is obtained

$$\frac{\partial^2 p^{n+1}}{\partial x_i \partial x_i} = \frac{\rho}{\Delta t \alpha} \frac{\partial \bar{u}_{i,f}^*}{\partial x_i}. \tag{8}$$

The numerical procedure at each time step can be summarized as follows:

1. Solve the discretized filtered Navier-Stokes equation for $\bar{u}$, $\bar{v}$ and $\bar{w}$.

2. Create an intermediate velocity field $\bar{u}_i^*$ from Eq. 7.

3. The Poisson equation (Eq. 8) is solved with an efficient multigrid method [13].

4. Compute the face velocities $\bar{u}_{i,f}^{n+1}$ (which satisfy continuity) from the pressure and the intermediate velocity as

$$\bar{u}_{i,f}^{n+1} = \bar{u}_{i,f}^{*} - \frac{1}{\rho}\alpha\Delta t \left(\frac{\partial p^{n+1}}{\partial x_i}\right)_f . \tag{9}$$

5. Step 1 to 4 is performed until convergence (normally one to three iterations) is reached.

6. The turbulent viscosity is computed.

7. Next time step.

Please note that although no explicit dissipation is added to prevent odd-even decoupling, an implicit dissipation is present. The intermediate velocity field is computed at the *nodes* (see Eq. 7) by subtracting a pressure gradient. Then, after having solved the pressure Poisson equation, the face velocity field is computed adding a pressure gradient at the *faces* (see Eq. 9). Thus a term is added, which is the difference between the pressure gradient at the face and the node. It can readily be shown that this term is proportional to the third derivative of pressure, i.e. $\partial^3 p/\partial x_i^3$ [14]. This term corresponds to Rhie-Chow dissipation [15].

4 Results

Below the two quantities ν_T and k_T are frequently used. Please recall that they are defined as follows: for $y \leq y_{ml}, \nu_T = \nu_t, k_T = k$, otherwise $\nu_T = \nu_{sgs}, k_T = k_{sgs}$.

4.1 Channel Flow

Figure 2a shows the predicted $\langle\bar{u}\rangle$ velocity ($\langle.\rangle$ denotes averaging over x, z and t) for fairly coarse meshes, see Table 1. A $32 \times 64 \times 32$ (x, y, z) grid is used. It can be seen that, for Case 2, in which the matching line is located at $y^+ = 60$, and $\Delta z^+ = 104$, the agreement with LES of Piomelli [6] is encouraging. However, a small kink is visible in the $\langle\bar{u}\rangle$ near the location of the matching line. When the resolution is made coarser in the spanwise direction (Case 3) the agreement with the benchmark LES becomes somewhat poorer. Note that the grid for Case 1, 2 & 3 is much coarser than that required for a wall-resolved LES. Consequently, when only LES is used (Case 4), the results are much poorer than those obtained with the hybrid LES–RANS model.

Figure 2b presents the predicted resolved, rms fluctuations. The agreement with benchmark LES is not good. The predictions are typical of an under-resolved LES: the streamwise fluctuations are too large, and the wall-normal and spanwise fluctuations are too small. It should be noted that the resolved stresses are large even in the RANS region.

4.2 Hill Flow

The configuration of the hill flow is shown in Fig. 1b. A $104 \times 64 \times 32$ (x, y, z) grid is used. The matching line along the lower wall is fixed to grid line number 13, so that

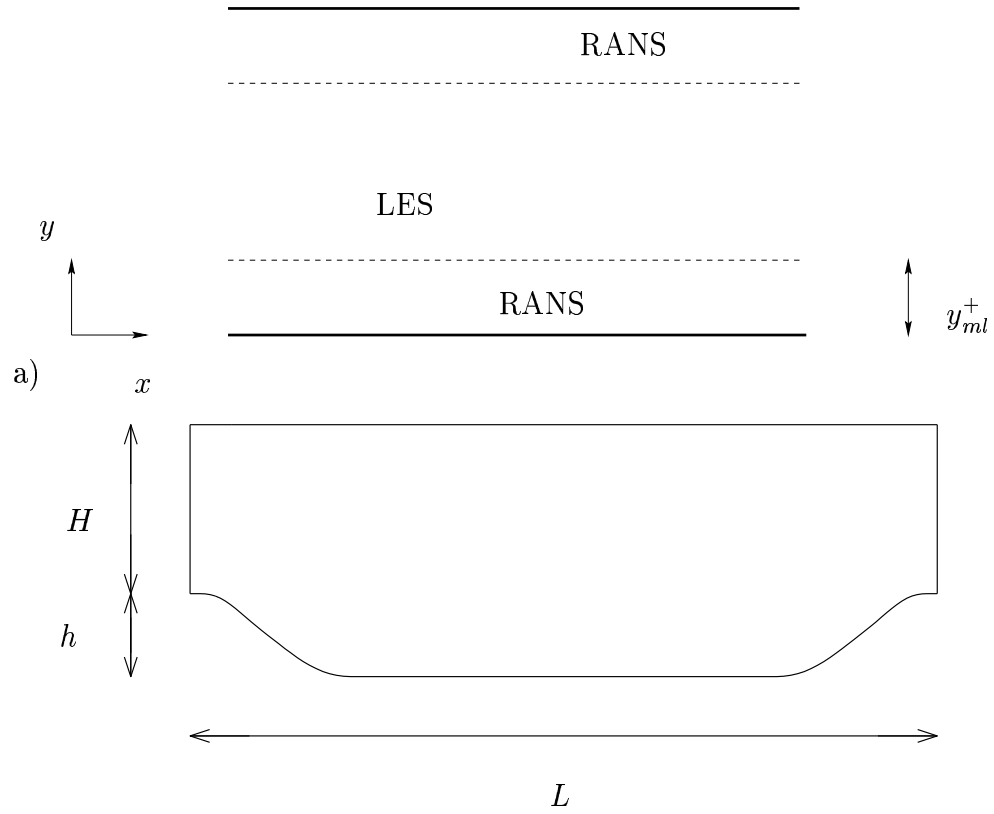

Figure 1: a) The near-wall RANS region and the outer LES region. b) Hill-flow configuration. $Re_b = U_b h/\nu \simeq 15\,800$, $\nu = 5 \cdot 10^{-6}$, $h = 0.028$, $H = 0.057$, $L = 9h$, $z_{max} = 9h$, U_b denotes the bulk velocity at the hill, i.e. at $x = 0$ and $x = L$.

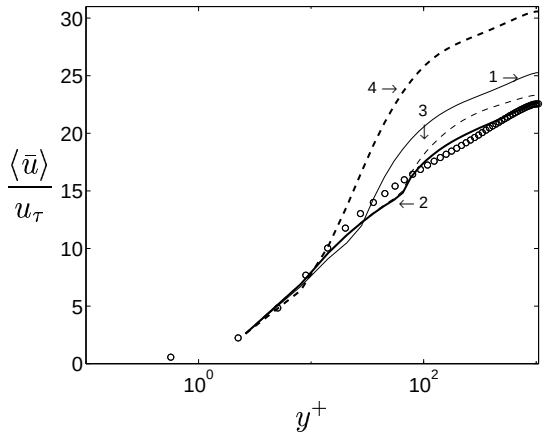

(a) Thin solid line: Case 1; thick solid line: Case 2; thin dashed line: Case 3; thick dashed line: Case 4.

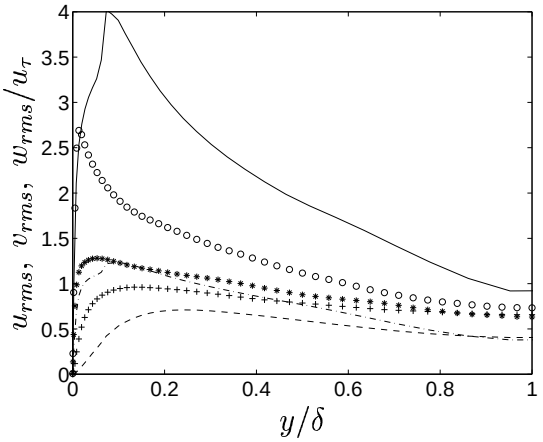

(b) Case 2. Resolved, rms fluctuations.

Figure 2: Channel flow. Markers: benchmark LES [6].

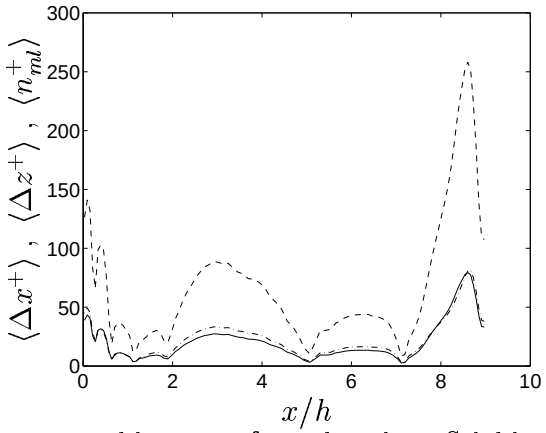

Figure 3: Hill flow. Grid spacing and location of matching line. Solid line: $\langle \Delta x^+ \rangle$; dashed line: $\langle \Delta z^+ \rangle$; dash-dotted line: $\langle n_{ml}^+ \rangle$.

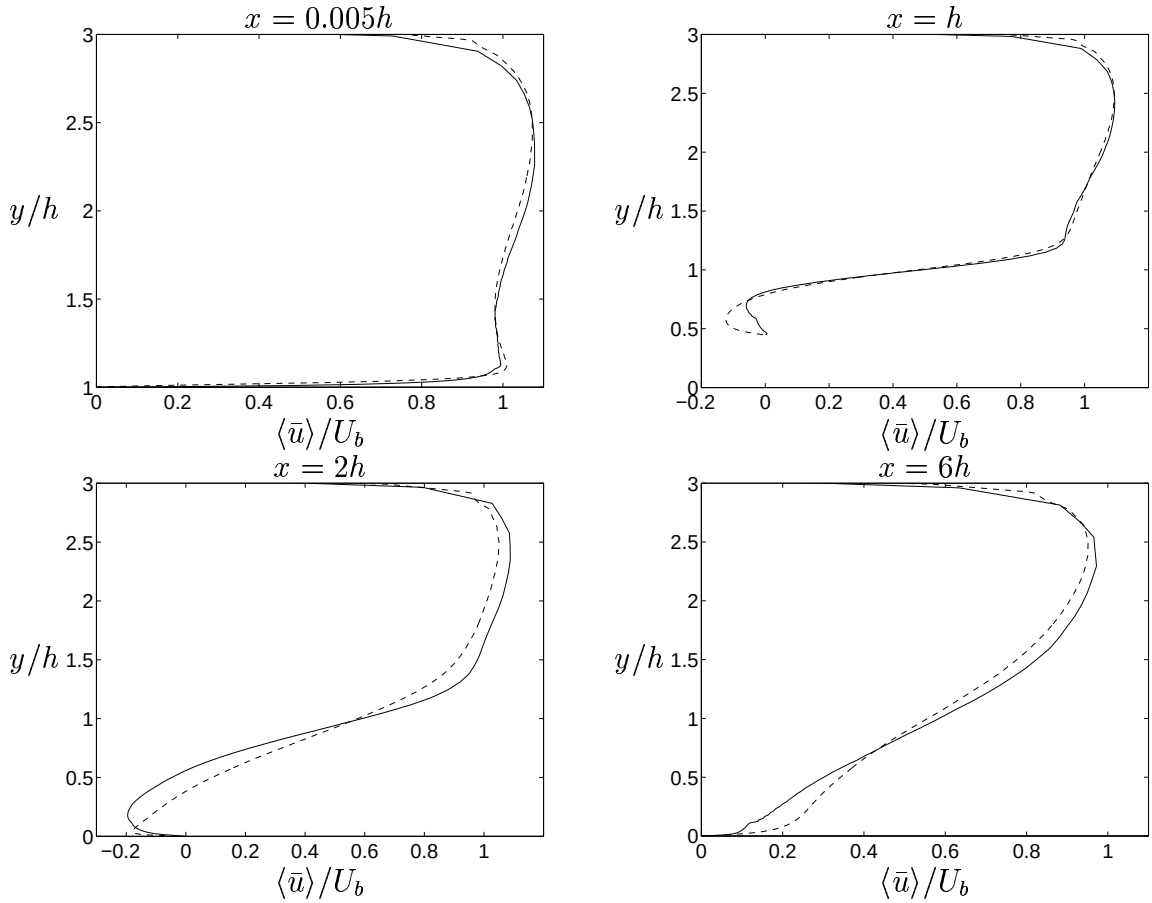

Figure 4: Hill flow. $\langle \bar{u} \rangle$ profiles. Solid lines: hybrid LES-RANS; dashed lines: benchmark LES [7, 8].

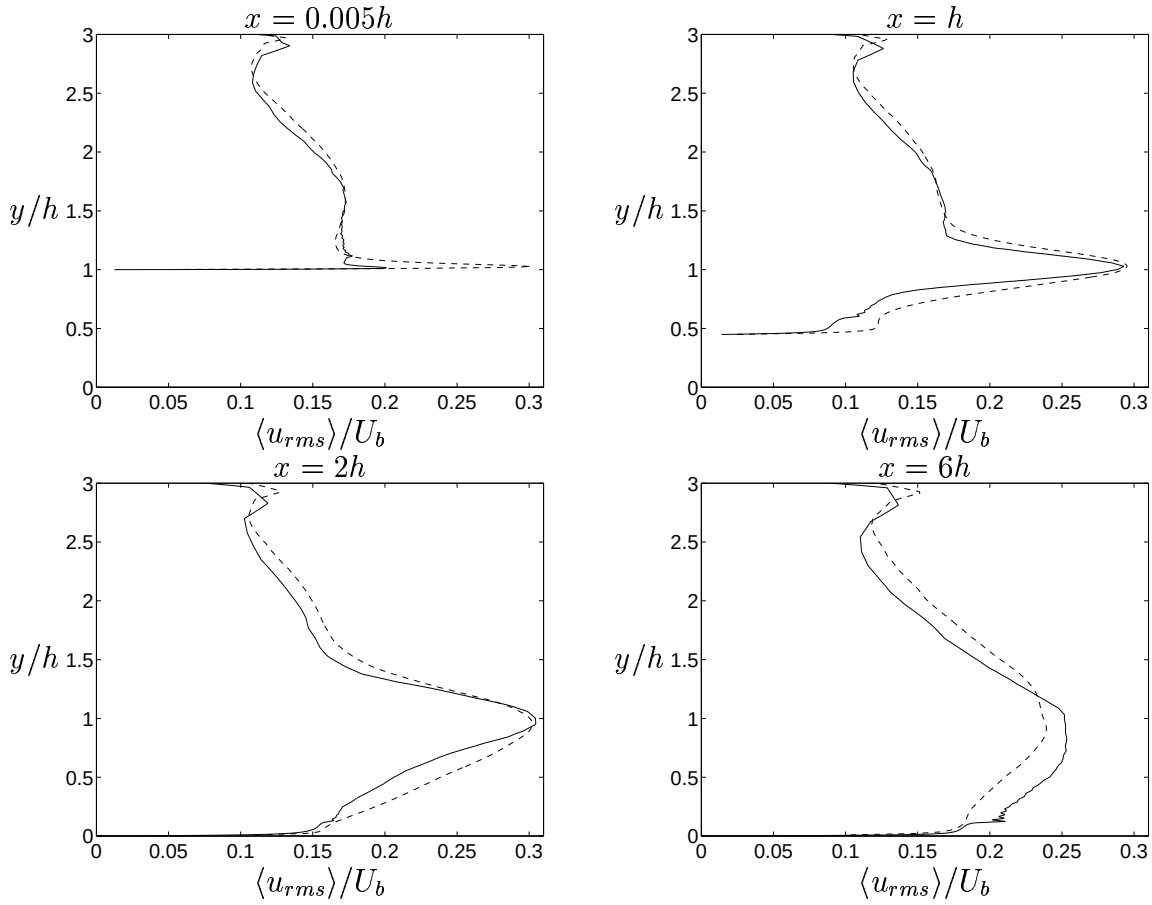

Figure 5: Hill flow. $\langle u_{rms} \rangle$ profiles. Solid lines: hybrid LES-RANS; dashed lines: benchmark LES [7, 8].

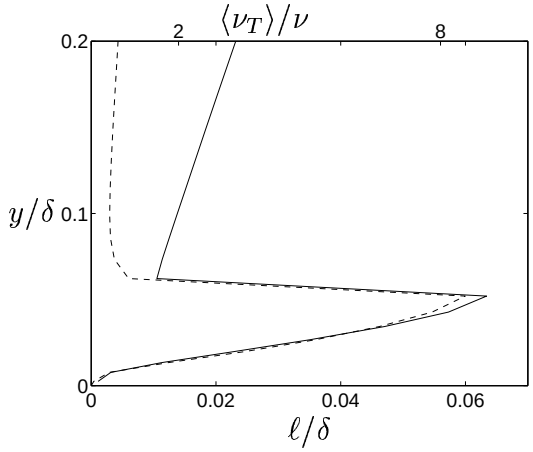

(a) Dashed line: RANS/SGS turbulent viscosity. Solid line: RANS/SGS turbulent length scales, $\ell = \langle\nu_T\rangle/(C_k\langle k_T\rangle^{1/2})$.

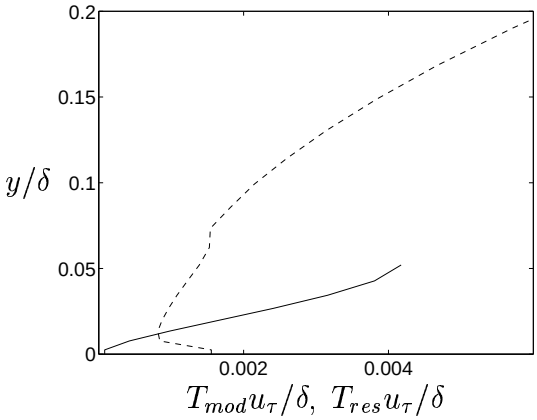

(b) Solid line: modelled turbulent time scale $u_\tau/(\delta\langle\omega\rangle)$; dashed line: resolved turbulent time scale $u_\tau\Delta/(\delta\langle k_{res}\rangle^{1/2})$.

Figure 6: Channel flow, Case 2. Near-wall region. Turbulent RANS/SGS time and length scales, and turbulent RANS/SGS viscosity.

the location of the matching line is at $\langle n_{ml}\rangle/h = 0.1 \pm 0.02$. No RANS region is used along the upper wall, but the LES region extends up to the wall. The cell size in x and z together with the location of the matching line (all in wall units) are shown in Fig. 3. As can be seen, high local values in $\langle\Delta x^+\rangle$ and $\langle\Delta z^+\rangle$ occur above the crest, while $\langle\Delta x^+\rangle \simeq \langle n_{ml}^+\rangle \lesssim 30$ and $\langle\Delta z^+\rangle \lesssim 100$ in the rest of the flow domain. For the nodes adjacent to the lower wall, $\langle y^+\rangle \lesssim 2$. The predictions are compared with a benchmark LES [7, 8] using more than 5 million cells.

Figures 4 and 5 compare the predicted $\langle\bar{u}\rangle$ velocity ($\langle.\rangle$ denotes averaging over z and t) and resolved, rms fluctuations with benchmark LES. The agreement is fairly good. As can be seen from the profiles at $x = h$ and $x = 2h$, the separation region with the hybrid LES-RANS model is slightly too strong. However, this is probably not due to the near-wall treatment. Instead it is believed to be a result of the shear layer emanating from the top of the hill being insufficiently resolved. Small kinks are seen – hardly visible – in the $\langle\bar{u}\rangle$ profiles close to the location of the matching line. These kinks are much smaller than found in the channel flow (cf. Fig. 2). The reason for this is probably that, in the hill flow, the convective and diffusive transport across the matching line is considerable, which has a smoothening effect on the flow quantities.

4.3 Discussion

The turbulent RANS/SGS viscosities are shown in Figs. 6a and 7a. It can be seen that the turbulent RANS viscosities are large in the RANS region – much larger than is

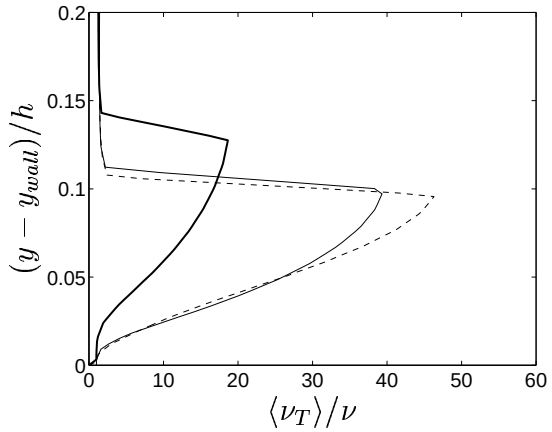

(a) Turbulent RANS/SGS viscosity.

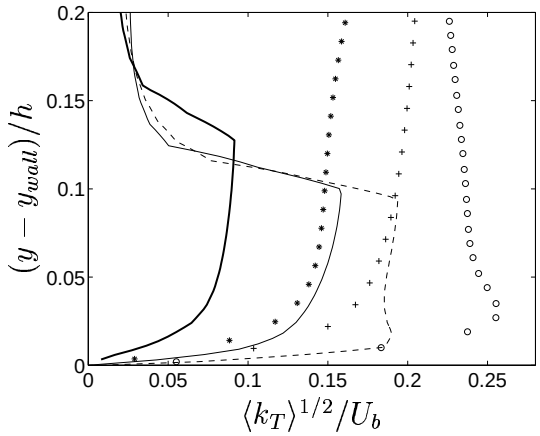

(b) Modelled turbulent RANS/SGS kinetic energy.

Figure 7: Hill flow. Near-wall region. Dashed line, o: $x/h = 0.005$; thick solid line, $*$: $x/h = 1$; thin solid line, $+$: $x/h = 6$. Markers: benchmark LES [7, 8].

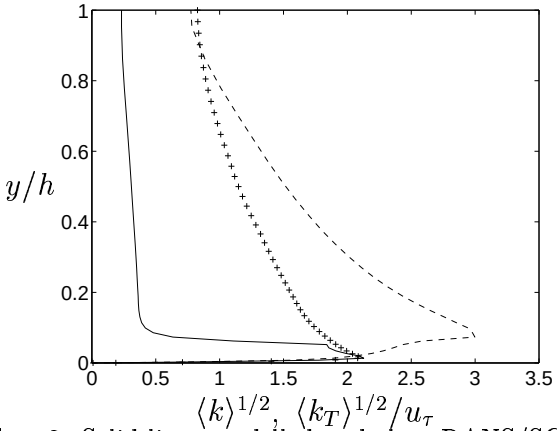

Figure 8: Channel flow, Case 2. Solid line: modelled turbulent RANS/SGS kinetic energy; dashed line: resolved turbulent kinetic energy; dashed lines: benchmark LES [6].

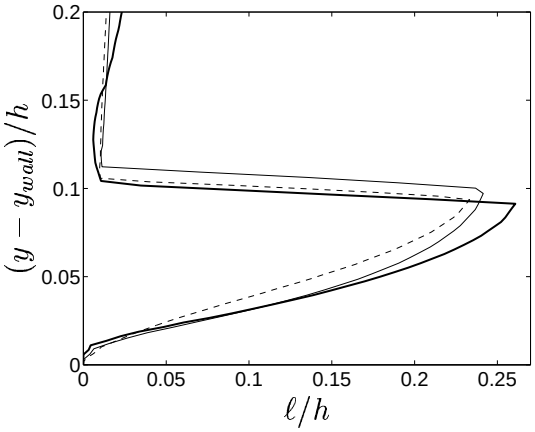

(a) Turbulent modelled length scale $\ell = \langle\nu_T\rangle/(C_k\langle k_T\rangle^{1/2})$. Dashed line: $x/h = 0.005$; thick solid line: $x/h = 1$; thin solid line: $x/h = 6$.

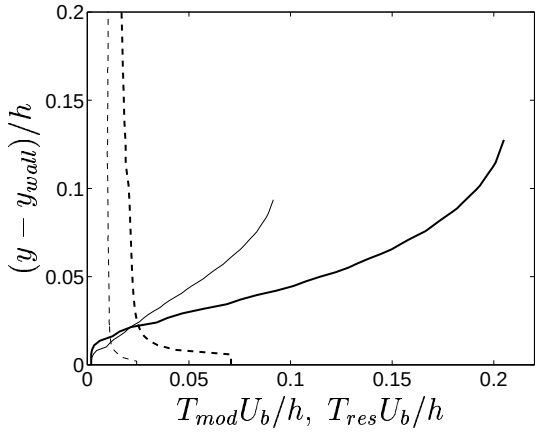

(b) Solid lines: turbulent modelled time scale $U_b/(h\langle\omega\rangle)$; dashed lines: resolved turbulent time scale $U_b\Delta/(h\langle k_{res}\rangle^{1/2})$. Thin lines: $x/h = 0.005$; thick lines: $x/h = 1$.

Figure 9: Hill flow. Near-wall region.

normally found in LES. Near the matching line, ν_{sgs} in the LES region drops down to typical SGS values of $2 \leq \langle\nu_{sgs}\rangle/\nu \leq 4$. The maximum value of ν_t (Fig. 6a) in the RANS region, which occurs near the matching line, is $\langle\nu_{t,max}\rangle/\nu \simeq 9$. When 1D, steady RANS is used to compute the channel flow using the same grid and the same $k-\omega$ model, the value of ν_t at the same location is approximately twice as large. One of the reasons why the RANS calculation gives larger ν_t values than the hybrid LES-RANS, is that in the former case more modelled, turbulent, kinetic energy is generated in the outer part of the logarithmic region ($y^+ > 60$). This is transported towards the wall by turbulent diffusion. Another reason is that in the hybrid LES-RANS computations, a substantial part of the turbulence in the RANS region is represented by resolved turbulence, see Fig. 2b.

Figures 7b and 8 show the modelled, turbulent RANS/SGS kinetic energy. For the channel flow, the modelled RANS kinetic energy agrees with the benchmark values. However, the resolved kinetic energy is as large as the modelled one in the RANS region. Therefore, the total kinetic energy (sum of modelled and resolved) is much too large. In the hill flow (Fig. 7b), the turbulent RANS kinetic energy is not that large. It is largest above the crest of the hill. This is probably due to the incorrect behavior of eddy-viscosity turbulence models, which due to the term $(\nu_t(\partial\bar{u}/\partial x)^2 > 0)$ predict positive production in accelerating flow, whereas the exact term is negative $(-\overline{u^2}\partial\bar{u}/\partial x < 0)$. Comparing k_T with the benchmark data, it can be seen that k_T is especially small in the recirculation region ($x/h = 1$). When a 2D RANS computation is performed with the same grid and the same $k-\omega$ model, the modelled, turbulent kinetic energy is up to 50% larger

compared to the hybrid LES-RANS data in Fig. 7b, but still smaller that the benchmark data. The reason why k is higher in a 2D RANS computation is, as noted in the channel flow computations, that turbulent kinetic energy is generated in the outer region which is diffused into the near-wall region.

Figures 6a and 9a give the modelled, turbulent length scales. The modelled turbulent RANS/SGS viscosity can be defined as $\nu_T \propto \mathcal{U}\ell$, where $\mathcal{U}$ and ℓ represent a turbulent RANS (SGS) velocity scale and length scale in the RANS (LES) region, respectively. In the LES region, the SGS length scale is $\ell = \Delta \equiv \nu_{sgs}/(C_k k_{sgs}^{1/2})$, see Eq. 4. In order to compare the turbulent RANS and the SGS length scales, the turbulent length scale is defined in the same way, so that $\ell = \nu_T/(C_k k_T^{1/2})$ in both the RANS and the LES region. As can be seen in Figs. 6a and 9a, the turbulent RANS/SGS length scale decreases steeply from the RANS region to the LES region. This decrease in the turbulent length scale from the RANS region to the LES region is the main reason for the decrease in the turbulent viscosity (Figs. 6a and 7a) and the turbulent RANS/SGS turbulent kinetic energy (Figs. 7b and 8).

In unsteady RANS, there should be a scale separation between the modelled time scale, T_{mod}, and the resolved time scale, T_{res}, so that $T_{mod} \ll T_{res}$. In the RANS region, the turbulent viscosity is computed as $\nu_t = k/\omega$, and thus the modelled time scale can be defined as $T_{mod} = 1/\omega$. The highest resolved time scale is related to the resolved turbulence and the smallest length scale, and it can be defined as $T_{res} = \min\{\Delta_\xi, \Delta_\eta, \Delta_\zeta\}/\langle k_{res}\rangle^{1/2} = \Delta/\langle k_{res}\rangle^{1/2}$, where k_{res} is the resolved, turbulent kinetic energy. The modelled and the resolved time scales are compared in Figs. 6b and 9b. As can be seen, the modelled time scale close to the wall is indeed smaller than the resolved one. However, in the larger part of the RANS region, the situation is the reverse: the modelled time scale is *larger* than the resolved one. Thus, formally, it is not correct to carry out an unsteady RANS. Indeed, it would be more correct to denote the near-wall region a VLES region rather. The SGS length scale in the VLES region is then $\ell = \nu_t/(C_k k^{1/2})$, which is presented in Figs. 6a and 9a. Note that if the wall region is redefined from a RANS region to a VLES region, it does not have any implications in the finite volume code: *it remains the same.*

There may also be some questions in defining the inner region as a VLES region. In this case, it may well happen that our SGS length scale, ℓ, becomes much larger than the filter size, Δ. Is that acceptable? The answer is probably that it depends on *how* much larger. In Smagorinsky models, the SGS length scale is chosen as the cubic root of the cell volume. Near walls this is much larger than the smallest cell side. However, if the SGS length scale becomes *very much* larger than Δ, it may perhaps be necessary to increase the filter size, i.e. do explicit filtering. This adds high complexity to the computations, especially since Δ would in general not be an even multiple of any cell width. A further complication is that the filter width would not be a function only of the space coordinates but also of time, i.e. $\Delta = \Delta(x_i, t)$. Thus there would be a commutation error in the time-derivative term in all equations, because the filter function would be a function of both space and time, i.e. $G = G(x_i, t)$.

5 Conclusions

A hybrid LES-RANS model is presented. In the near-wall region, RANS is used and the turbulence modelled with a $k-\omega$ model. LES is used in the outer region and the SGS turbulence is modelled with a one-equation SGS k_{sgs} model. The matching line is in the inner part of the logarithmic region. The main idea is that it is not necessary with this new model to resolve the near-wall streaks in the viscous and the buffer layer. Instead these are modelled in the same way as in standard RANS. However, the large, turbulent scales in the outer region ($y^+ \gtrsim 60$) are resolved by the LES.

The hybrid LES-RANS model has been applied to fully developed channel flow and the hill flow. The mean flow is fairly well predicted with a coarse mesh, both for the channel flow and the hill flow. Kinks in the velocity profiles are observed in the region of the matching line. However, this problem is much smaller in the hill flow. The reason is probably that the transport of mass and momentum across the matching line by convection and turbulent diffusion has a smoothening effect. One way to further reduce the gradients across the matching line could be to use some kind of smoothing function as Strelets [16] proposes.

5.1 Acknowledgments

This work was financed by the LESFOIL project (no. BE97-4483) in the Brite-Euram programme. Computer time at the SGI ORIGIN 2000 machines at UNICC, Chalmers, is gratefully acknowledged.

[1] postscript file at http://www.tfd.chalmers.se/~lada

REFERENCES

[1] U. Piomelli and J.R. Chasnov. Large-eddy simulations: Theory and applications. In D. Henningson, M. Hallbäck, H. Alfredsson, and A. Johansson, editors, *Transition and Turbulence Modelling*, pages 269–336, Dordrecht, 1996. Kluwer Academic Publishers.

[2] N.V. Nikiton, F. Nicoud, B. Wasistho, K.D. Squires, and P. Spalart. An approach to wall modeling in large-eddy simulations. *Physics of Fluids A*, 12(7):1629–1632, 2000.

[3] P.R. Spalart, W.-H. Jou, M. Strelets, and S.R. Allmaras. Comments on the feasability of LES for wings and on a hybrid RANS/LES approach. In C. Liu and Z. Liu, editors, *Advances in LES/DNS, First Int. conf. on DNS/LES*, Louisiana Tech University, 1997. Greyden Press.

[4] M. Shur, P.R. Spalart, M. Strelets, and A. Travin. Detached-eddy simulation on an airfoil at high angle of attack. In W. Rodi and D. Laurence, editors, *Engineering Turbulence Modelling and Experiments 4*, pages 669–678. Elsevier, 1999.

[5] A. Travin, M. Shur, M. Strelets, and P. Spalart. Detached-eddy simulations past a circular cylinder. *Flow Turbulence and Combustion*, 63(1/4):293–313, 2000.

[6] U. Piomelli. High Reynolds number calculations using the dynamic subgrid-scale stress model. *Physics of Fluids A*, 5:1484–1490, 1993.

[7] C. Mellen, J. Fröhlich, and W. Rodi. Karlruhe's mid-term report, LESFOIL: A Brite-Euram project. Technical report, Institut für Hydrodynamik, University of Karlsruhe, Germany, 1999.

[8] C.P. Mellen, J. Frölich, and W. Rodi. Large eddy simulation of the flow over periodic hills. In *16th IMACS World Congress 2000, Lausanne, August 21-25*, 2000.

[9] S-H Peng, L. Davidson, and S. Holmberg. A modified low-Reynolds-number $k-\omega$ model for recirculating flows. *ASME: Journal of Fluids Engineering*, 119:867–875, 1997.

[10] A. Yoshizawa. Bridging between eddy-viscosity-type and second-order models using a two-scale DIA. In *9th Int. Symp. on Turbulent Shear Flow*, volume 3, pages 23.1.1—23.1.6, Kyoto, 1993.

[11] C. Fureby. Large eddy simulation of rearward-facing step flow. *AIAA Journal*, 37(11):1401–1410, 1999.

[12] L. Davidson and S.-H. Peng. A hybrid LES–RANS model based on a one-equation SGS model and a two-equation $k-\omega$ model. In *The Second International Symp. on Turbulence and Shear Flow Phenomena*, Stockholm, 2001.[1]

[13] P. Emvin. *The Full Multigrid Method Applied to Turbulent Flow in Ventilated Enclosures Using Structured and Unstructured Grids*. PhD thesis, Dept. of Thermo and Fluid Dynamics, Chalmers University of Technology, Göteborg, 1997.

[14] L. Davidson. MTF071 Computational Fluid Dynamics of turbulent flow. Lecture notes, www.tfd.chalmers.se/gr-kurs/MTF071, Dept. of Thermo and Fluid Dynamics, Chalmers University of Technology, Göteborg, Sweden, 2000.

[15] C.M. Rhie and W.L. Chow. Numerical study of the turbulent flow past an airfoil with trailing edge separation. *AIAA Journal*, 21:1525–1532, 1983.

[16] M. Strelets. Detached eddy simulation of massively separated flows. AIAA paper 2001–0879, Reno, NV, 2001.